JOURNAL OF MATERIALS SCIENCE 35 (2000) 5809–5816

Bulk permittivity of a composite with coated spheroidal filler particles

N. HARFIELD
Center for Nondestructive Evaluation, Iowa State University, 1915 Scholl Road, Applied Sciences Complex II, Ames, IA 50011-3042, USA
E-mail: nicola@cnde.iastate.edu

The bulk complex permittivity of a composite material is calculated analytically. The filler particles are spheroidal and may be coated with a surface layer whose intrinsic material properties differ from those of the core. Making the assumption that the filler particles are arranged on a simple-cubic lattice, interactions between the particles are accounted for by treating each particle mathematically as a multipole source. The coefficients of the multipole expansion, suitably-truncated, are determined by solving a matrix equation obtained by matching with the general solution of Laplace's equation in the interstitial domain, expressed in terms of an expansion in spheroidal harmonics. Matching is carried out at the surface of a representative particle according to electromagnetic continuity conditions. Example calculations demonstrate the effect of varying filler volume fraction, intrinsic material properties, layer thickness, particle shape and frequency. Results are shown to agree with independent work, where available.

1. Introduction

Composite materials have numerous applications that exploit their electromagnetic properties. These applications include static shielding of delicate electronic components and radar absorption. It is useful to be able to predict the bulk behavior of a composite from knowledge of the intrinsic properties of its constituents, since this ability is a fundamental requirement in the efficient design of novel materials. There is mathematical equivalence in the calculation of a number of physical parameters including electrical and thermal conductivity, dielectric permittivity and magnetic permeability [1]. This fact has been partly responsible for the rich abundance of contributions on the subject, as workers in many fields have addressed the problem of calculating the properties of a material with more than one phase. Hence, the works cited by this paper are motivated by problems in thermal and electrical conduction, and in fluid mechanics. The numerous methods which abound all have to take into account the relative spatial distributions of the phases in some way.

In this work, filler particles in a matrix are assumed to occupy the sites of a simple-cubic lattice. This regular spatial arrangement permits calculation of the bulk complex dielectric permittivity to be predominantly analytic [2, 3]. Particles are considered to be spheroidal in shape and may be coated with a surface layer whose intrinsic properties differ from those of the core. Modeling a coated particle has practical relevance in a number of ways. For example, it is often desirable to enhance the electrical conductivity of a polymer matrix by loading it with metal particles, but this has the effect of increasing the density and weight of the resulting composite, which is a disadvantage for many applications. A thin metal layer deposited on a low-density particle may perform as well electrically as a similar but solid metal particle, depending on the frequency of operation, but with the advantage of much reduced weight [4]. A thin surface layer may also be used in practice to improve wetting of the filler by the matrix material and, conversely, the effect of imperfect bonding between the particle and matrix phases can be simulated by a layer with suitable properties [5].

The work presented here will be confined to spheroids whose axes of rotation are aligned with each other and with one of the lattice vectors, although the method of solution lends itself to treat spheroids arbitrarily oriented with respect to the lattice [6]. Also, a single layer coating the filler particles will be considered here, but a straightforward extension of the analysis would give the solution for multiple layers. A further extension, in which more than one particle can be positioned within the unit cell of the simple-cubic lattice [7], is feasible and permits modeling of composites with distributions of filler particle size, shape and orientation, with a variety of spatial distributions.

The following section of this paper contains the theoretical development. In Section 3, results of some example calculations are presented in which the effect of varying the filler volume fraction (f), intrinsic material properties of the phases, layer thickness, particle shape and frequency are examined. Good agreement with independent work is shown.

2. Theory

The theoretical basis of this work has been given in detail elsewhere [6, 8] in the context of calculation of the bulk electrical conductivity of a two-phase composite, so a brief summary will be given here, with closer attention paid to calculation of the complex permittivity and treatment of the surface layer on the filler particles.

2.1. Field equations

Begin with the well-known Maxwell-Ampère Law:

$$\nabla \times H = J + \frac{\partial D}{\partial t} \tag{1}$$

where H is the magnetic field, J is the current density and D is the displacement current. Now assume that the system behaves linearly and that the following linear macroscopic constitutive relations with the electric field E can be written:

$$\langle J \rangle = \overline{\overline{\sigma}} \cdot \langle E \rangle \tag{2}$$

$$\langle D \rangle = \epsilon_0 \overline{\overline{\epsilon}}' \cdot \langle E \rangle. \tag{3}$$

Above, the angled braces denote macroscopic values, ϵ_0 is the permittivity of free space and $\overline{\overline{\sigma}}$ and $\overline{\overline{\epsilon}}'$ are second-order tensors describing the bulk conductivity and real permittivity respectively. Assuming that the excitation is time-harmonic, with behavior $\exp(-i\omega t)$, the Maxwell-Ampère law implies that

$$\nabla \times \langle H \rangle = -i\omega\epsilon_0 \overline{\overline{\epsilon}} \cdot \langle E \rangle \tag{4}$$

where the complex permittivity is defined

$$\overline{\overline{\epsilon}} = \overline{\overline{\epsilon}}' + i\overline{\overline{\epsilon}}'' \tag{5}$$

with

$$\overline{\overline{\epsilon}}'' = \frac{\overline{\overline{\sigma}}}{\omega\epsilon_0}. \tag{6}$$

In the following development, $\overline{\overline{\epsilon}}$ is the quantity which will be determined.

For a material consisting of spheroids arranged on the nodes of a simple-cubic lattice such that their axes of rotation coincide with one of the lattice vectors, shown in Fig. 1, there are only two independent components of $\overline{\overline{\epsilon}}$:

$$\overline{\overline{\epsilon}} = \begin{pmatrix} \epsilon_{xx} & 0 & 0 \\ 0 & \epsilon_{xx} & 0 \\ 0 & 0 & \epsilon_{zz} \end{pmatrix}. \tag{7}$$

This means that $\overline{\overline{\epsilon}}$ can be found by solving two similar scalar problems in which a unit electric field is applied parallel to x, giving ϵ_{xx}, and parallel to z, giving ϵ_{zz}.

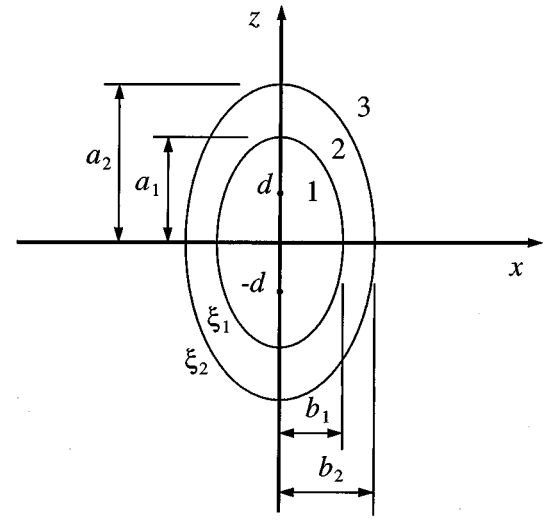

Figure 1 Cross-section of a coated prolate spheroid with axis of rotation parallel to z. Domain 1 is the particle core, domain 2 is the particle layer and the interstitial domain is denoted by 3.

2.2. Electric potential

Define the local electric potential Φ_i in terms of the local electric field as follows:

$$E_i(\mathbf{r}) = -\nabla\Phi_i(\mathbf{r}). \tag{8}$$

The above definition assumes a non-magnetic material, i.e.

$$\nabla \times E_i(\mathbf{r}) = 0.$$

The subscript $i = 1$ denotes the particle core domain, $i = 2$ the particle layer domain, $i = 3$ the interstitial domain and $\mathbf{r}$ is the position vector. Applying constitutive relations (2) and (3) locally and substituting into (1) with (8) shows that the electric potential obeys the Laplace equation everywhere in the material,

$$\nabla^2\Phi_i(\mathbf{r}) = 0, \quad i = 1, 2, 3. \tag{9}$$

Applying a uniform electric field $\langle E \rangle$, the potential at any position in the composite can be expressed

$$\Phi_i(\mathbf{r}) = \breve{\Phi}(\mathbf{r}) - \mathbf{r} \cdot \langle E \rangle \tag{10}$$

where $\breve{\Phi}$ is a spatially periodic function

$$\breve{\Phi}(\mathbf{r}) = \breve{\Phi}(\mathbf{r} + \mathbf{r}_n) \tag{11}$$

and the set of vectors $\mathbf{r}_n$ locate the nodes of the lattice at which the particles are positioned.

2.3. Particles as multipoles

Equation 9 can be solved by replacing the particles by singular multipole source distributions located at their centers, analytically continuing the interstitial fields into the space occupied by the particles. A low-order solution of this problem, valid for volume fractions up to about 30%, may be obtained by assuming that each particle behaves as a dipole field source. This approach

was adopted by Maxwell in 1881 [9] and leads to a solution which does not account for particle-particle interaction. To take these interactions into consideration and to deal with non-spherical particles, higher-order multipoles are required. The contribution to the field from all particles is obtained by summing over the lattice sites, following a Fourier method due to Hasimoto [10]. As shown in references [6] and [8], the following expression can be established:

$$\breve{\Phi} = \Phi_0 - \frac{1}{4\pi} B \nabla S \cdot \langle E \rangle, \tag{12}$$

in which Φ_0 is a constant potential, B is the partial differential operator

$$B = \sum_{m=0}^{\infty} \sum_{n=0}^{\infty} \sum_{p=0}^{\infty} b^{mnp} \frac{\partial^{2(m+n+p)}}{\partial x^{2m} \partial y^{2n} \partial z^{2p}} \tag{13}$$

and S is a periodic, singular solution of Laplace's equation which may be expressed

$$S = \frac{1}{r} - c + \frac{2\pi r^2}{3\tau_0} + \sum_{n=2}^{\infty} \sum_{m=0}^{m \le n/2} a_{nm} r^{2n} P_{2n}^{4m}(\cos\theta) \cos 4m\phi \tag{14}$$

In (14), c is a constant with value 2.8379297 [11], τ_0 is the volume of the unit cell and the P_n^m are Legendre functions of the first kind of degree n and order m. Further, r, θ, ϕ are the usual spherical co-ordinates originating at the center of the particle. Derivatives of increasing order in B correspond to multipoles of increasing order. Thus, the accuracy of the solution is determined by the number of terms retained on truncation of the series. To achieve a certain level of accuracy, more terms are required as a) the particle shape departs from being spherical and b) the difference between the material properties in each phase becomes greater. The expression of S in spherical harmonics allows Φ_3 also to be written as an expansion in spherical harmonics [6].

The coefficients b^{mnp} in (13) will be determined by applying electromagnetic conditions of continuity at the interfaces between regions 1, 2 and 3. As shown elsewhere [6], the transport coefficient which is sought can be readily determined from b^{000} using

$$\epsilon_{jj} = 1 - \frac{b_{jj}^{000}}{\tau_0}, \tag{15}$$

where $j = x$ or z. Analytic expressions for b_{xx}^{000} and b_{zz}^{000} up to order $f^{14/3}$ are quoted in the Appendix.

2.4. Interface conditions

At the interfaces between the core, layer and interstitial domains, the electromagnetic field obeys standard conditions of continuity [12]. Continuity of the tangential component of E leads to the requirement that the electric potential be continuous across the interfaces:

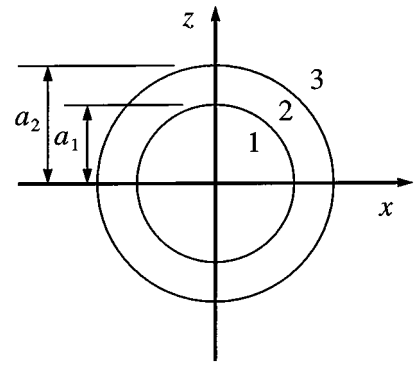

Figure 2 Cross-section of a coated sphere.

$$\Phi_i(\mathbf{r}_-) = \Phi_{i+1}(\mathbf{r}_+), \quad i = 1, 2 \tag{16}$$

where $\mathbf{r}_-$ and $\mathbf{r}_+$ denote points on the interface approached from regions i and $i+1$ respectively. Continuity of the normal component of $J + \partial D/\partial t$ leads to

$$\epsilon_i \frac{\partial \Phi_i(\mathbf{r})}{\partial N}\bigg|_{r=r_-} = \epsilon_{i+1} \frac{\partial \Phi_{i+1}(\mathbf{r})}{\partial N}\bigg|_{r=r_+}, \quad i = 1, 2 \tag{17}$$

where N is the co-ordinate normal to the interface and ϵ_1, ϵ_2 and ϵ_3 denote the intrinsic, homogeneous permittivities of the constituent phases. The conditions stated in (16) and (17) will now be applied to general harmonic expansion solutions of (9).

The general solution of (9) in terms of spherical harmonics, appropriate for the spherical particle shown in Fig. 2, is written

$$\Phi_1 = \sum_{n=0}^{\infty} \sum_{m=0}^{n} G_{nm} Y_n^m \tag{18}$$

$$\Phi_2 = \sum_{n=0}^{\infty} \sum_{m=0}^{n} \left(E_{nm} + F_{nm} r^{-2n-1}\right) Y_n^m \tag{19}$$

$$\Phi_3 = \sum_{n=0}^{\infty} \sum_{m=0}^{n} \left(C_{nm} + D_{nm} r^{-2n-1}\right) Y_n^m \tag{20}$$

where

$$Y_n^m = \frac{1}{(n-m)!} r^n P_n^m(\cos\theta) \cos m\phi.$$

The function Y_n^m, even with respect to ϕ, has an odd counterpart which is not required here due to the symmetry of the problem.

Applying conditions (16) and (17) to Equations 18 and 19 at the boundary between the particle core and layer, $r = a_1$, the F_{nm} can be eliminated and Φ_2 expressed

$$\Phi_2 = \sum_{n=0}^{\infty} \sum_{m=0}^{n} E_{nm} \left(1 + a_1^{2n+1} \mathcal{L}_n^{12} r^{-2n-1}\right) Y_n^m \tag{21}$$

with

$$\mathcal{L}_s^{12} = \frac{\rho_{12} - 1}{\rho_{12} + (s+1)/s} \tag{22}$$

and $\rho_{ij} = \epsilon_i/\epsilon_j$. Now eliminating the D_{nm} by applying the continuity conditions at the particle surface, $r = a_2$, gives

$$\Phi_3 = \sum_{n=0}^{\infty} \sum_{m=0}^{n} C_{nm}\left(1 + a_2^{2n+1}\mathcal{L}_n^{23} r^{-2n-1}\right) Y_n^m \tag{23}$$

with

$$\mathcal{L}_s^{23} = \frac{\rho_{23} g_s - 1}{\rho_{23} g_s + (s+1)/s}, \tag{24}$$

and

$$g_s = \frac{1 - [(s+1)/s](a_1/a_2)^{2s+1}\mathcal{L}_s^{12}}{1 + \mathcal{L}_s^{12}(a_1/a_2)^{2s+1}}. \tag{25}$$

In the case of spheroidal particles, a procedure similar to that outlined above is followed but now in terms of spheroidal harmonics with co-ordinate system

$$x = d\bar{\xi}\bar{\eta}\cos\phi$$
$$y = d\bar{\xi}\bar{\eta}\sin\phi$$
$$z = d\xi\eta$$

with

$$\bar{\xi}^2 = \xi^2 - 1 \text{ and } \bar{\eta}^2 = 1 - \eta^2.$$

The interfocal distance of the spheroid is $2d$ and surfaces of constant ξ define concentric spheroids. Applying interface conditions to the general harmonic expansion solutions of (9) gives

$$\Phi_3 = \sum_{n=0}^{\infty} \sum_{m=0}^{n} C_{nm}\left[P_n^m(\xi) + \mathcal{L}_{nm}^{23} Q_n^m(\xi)\right]\mathcal{Y}_n^m \tag{26}$$

where

$$\mathcal{Y}_n^m = P_n^m(\eta)\cos m\phi,$$

and

$$\mathcal{L}_{st}^{23} = -\frac{(\rho_{23}-1)P_s^t(\xi_2)P_s^t(\xi_2)' + \mathcal{L}_{st}^{12}\left[\rho_{23}P_s^t(\xi_2)Q_s^t(\xi_2)' - P_s^t(\xi_2)'Q_s^t(\xi_2)\right]}{\rho_{23}P_s^t(\xi_2)'Q_s^t(\xi_2) - P_s^t(\xi_2)Q_s^t(\xi_2)' + \mathcal{L}_{st}^{12}(\rho_{23}-1)Q_s^t(\xi_2)Q_s^t(\xi_2)'} \tag{27}$$

where

$$\mathcal{L}_{st}^{12} = -\frac{\rho_{12} - 1}{\rho_{12}\left[Q_s^t(\xi_1)/P_s^t(\xi_1)\right] - \left[Q_s^t(\xi_1)'/P_s^t(\xi_1)'\right]}. \tag{28}$$

The prime indicates the derivative normal to the surface, i.e.

$$L_s^t(\xi_i)' \equiv \left.\frac{dL_s^t(\xi)}{d\xi}\right|_{\xi=\xi_i}$$

with L either P or Q.

The above equations are in a form appropriate for prolate spheroids. The correct expressions for oblate spheroids are obtained directly from these equations by formally replacing ξ and $i\xi$ and d with $-id$.

Growing and decaying terms in (23) and (26) are now matched with terms in the multipole expansion and the resulting systems of linear equations solved to give the b^{mnp} in each case. With (26) there is an intermediate step in which the spheroidal harmonics are transformed to spherical harmonics [6, 8]. The bulk permittivity can then be calculated simply from (15), using results quoted in the Appendix.

3. Example calculations and discussion

In Fig. 3, the calculated complex permittivity is shown as a function of frequency for spherical particles with layers of different thickness. The value t given on the figure is the ratio of the layer thickness to the particle radius. The intrinsic material parameters used in the calculation are

$$\epsilon_1' = \epsilon_3' = 1$$
$$\epsilon_2' = 10$$
$$\sigma_1 = \sigma_3 = 0.00 \text{ S/m}$$
$$\sigma_2 = 0.01 \text{ S/m}$$

and the volume fraction $f = 0.4$. These parameters are chosen to facilitate comparison with results published independently [13], for the case $t = 1.0$ (homogeneous particle). The curves in Fig. 3a and b for $t = 1.0$ agree with the curve for the simple-cubic lattice of spheres given in Fig. 7a of [13]. As the layer thickness is reduced, the relaxation frequency falls; marked by the positions of the inflexion points in Fig. 3a and the positions of the maxima in Fig. 3b. This behavior is evidence of the interfacial, or Maxwell-Wagner, polarization mechanism. At frequencies above the relaxation frequency, the limiting value of the real permittivity, $\lim_{\nu\to\infty}(\epsilon') = \epsilon_\infty$, also falls as the layer thickness is reduced. This feature can be explained by noting that the polarization of each particle is mathematically equivalent to the effect of a certain distribution of volume and surface charge. As the layer thickness is reduced, the contribution from the volume charge distribution declines, since the particle core in this example is electrically inert, and ϵ_∞ declines. In Fig. 3b it can be seen

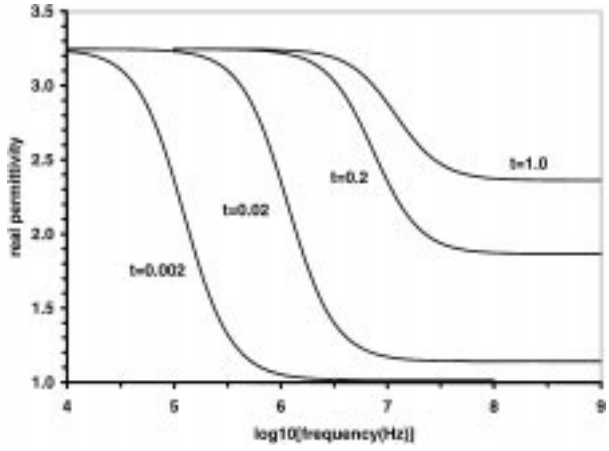

(a)

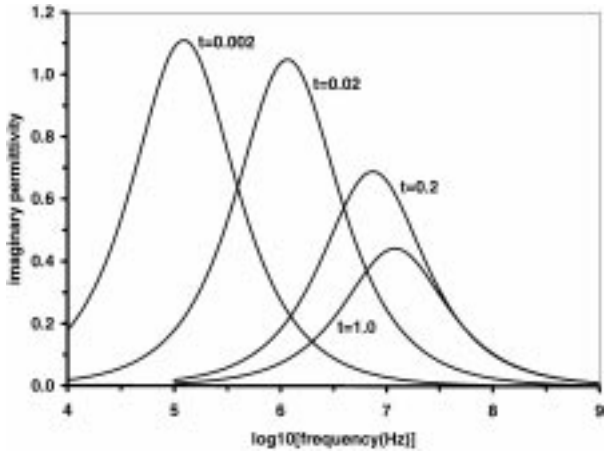

(b)

Figure 3 (a) Real and (b) imaginary parts of bulk permittivity for composite material with spherical filler particles, $f = 0.4$.

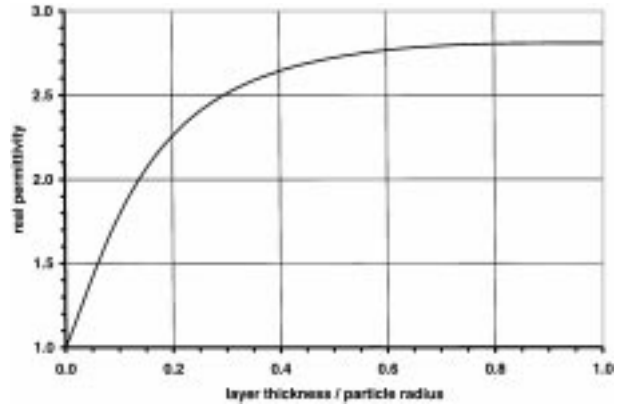

(a)

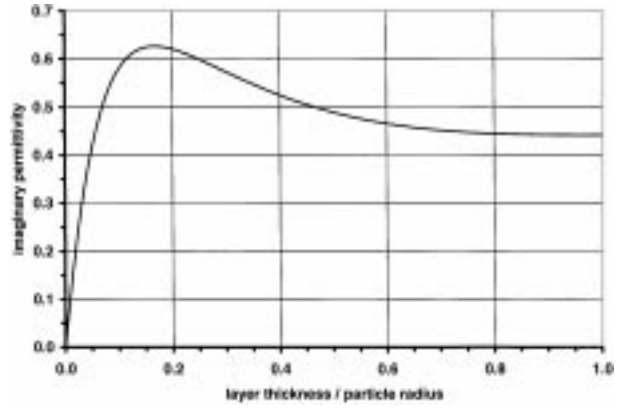

(b)

Figure 4 (a) Real and (b) imaginary parts of bulk permittivity for composite material with spherical filler particles, $f = 0.4$, at fixed frequency $\nu = 11.8$ MHz.

that the peak value of ϵ'' increases as the layer thickness is reduced, tending to a limiting value $(\epsilon_s - \epsilon_\infty)/2$ with $\epsilon_s = \lim_{\nu \to 0}(\epsilon')$. This shows that the system can be described in terms of a Debye theory of relaxation [14].

The curves in Fig. 4a and b show the effect of varying t at fixed frequency. Choosing the relaxation frequency for $t = 1.0$ of Fig. 3, $\nu = 11.8$ MHz, the layer thickness ranges from zero to full thickness. Clearly ϵ' increases monotonically as the layer thickness increases, whereas ϵ'' peaks at $t \approx 0.17$. This kind of observation may be useful in optimizing layer thickness to achieve maximum electromagnetic absorption at a particular frequency.

The way in which ϵ is affected by particle shape is shown in Fig. 5. The material parameter values are as for Fig. 3 with $t = 1.0$, but here the volume fraction is 0.1. Curves are shown for spheres, oblate spheroids with aspect ratio 0.2 and prolate spheroids with aspect ratio 2.0. The curves for spherical particles are similar to those for $t = 1.0$ in Fig. 3, with the same relaxation frequency, but the magnitude of ϵ' and ϵ'' is reduced due to the lower volume fraction. For the spheroids, results are plotted for the electric field applied both perpendicular (E_x) and parallel (E_z) to the axis of rotation. The oblate, disc-like particles demonstrate the strongest anisotropy, with large values of real and imaginary permittivity for x-directed applied electric field. This is because disc-like particles with aspect ratio 0.2 approach each other more closely at $f = 0.1$ than the other particles considered in Fig. 5, leading to large inter-particle capacitance. Note that there is a gradual reduction in the relaxation frequency as ϵ increases, due to these shape effects.

In Fig. 6, comparison is made with results of an equivalent-inclusion model for the bulk thermal conductivity of a composite with randomly-distributed particles [5]. The essence of the equivalent-inclusion method is that a layered particle, with different coefficients of thermal conductivity in the core and layer, is replaced by a homogeneous particle and a volume distribution of dipoles such that the equivalent inclusion induces the same temperature gradient as the coated particle. This assumption leads to the restriction that the results are valid for f up to approximately 0.4. Meaningful comparison with the simple-cubic lattice model is possible since the difference in microstructure only becomes evident for f greater than about 0.3. Calculation of thermal conductivity is equivalent to calculation of electrical conductivity, σ, or static permittivity ϵ'_s. It is thus possible to make predictions of thermal conductivity using the model presented above. The intrinsic material parameters are as for Fig. 7 in [5], representing a material composed of spherical diamond filler particles of average radius 2 μm dispersed in a ZnS matrix. The interfacial thermal resistance between the matrix and filler, 6×10^{-8} m^{2}K/W, was determined experimentally. Assuming an interfacial layer thickness of 1 nm on the semi-minor axis of the spheroid (i.e.

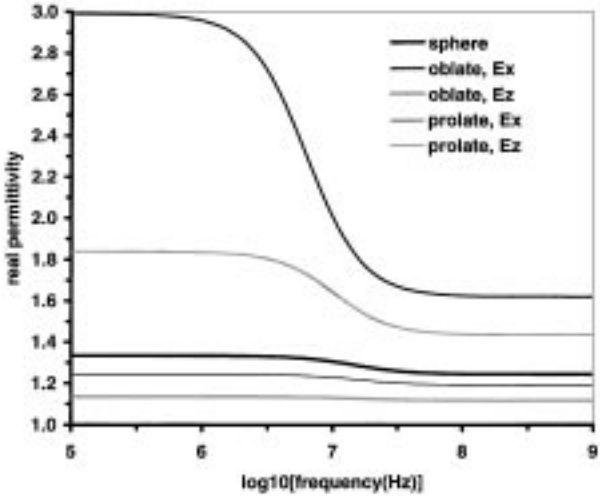

(a)

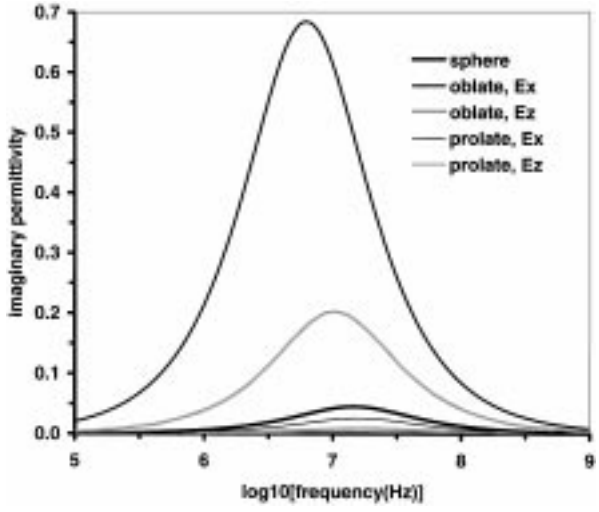

(b)

Figure 5 (a) Real and (b) imaginary parts of bulk permittivity for composite material with filler particles having aspect ratios 0.2, 1.0 and 2.0, and volume fraction $f = 0.1$.

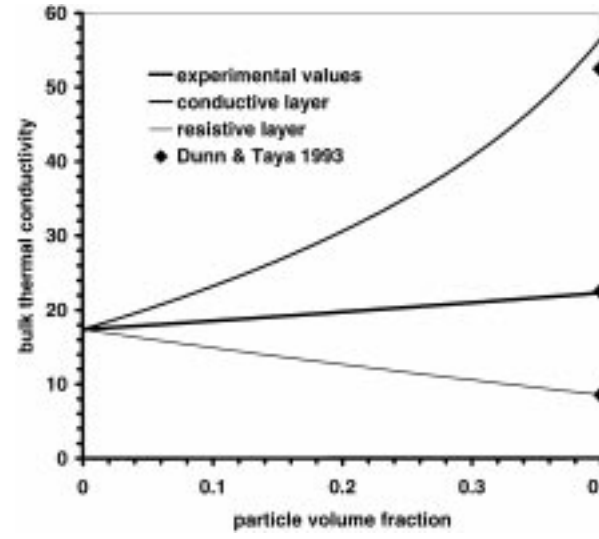

(a)

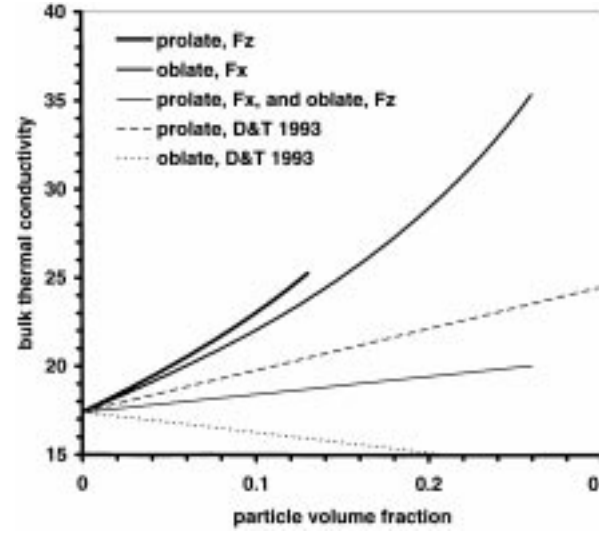

(b)

Figure 6 Bulk thermal conductivity for composite material with coated filler particles: (a) spherical and (b) spheroidal with aspect ratios 0.5 and 2.0.

$b_2 - b_1 = 1$ nm, see Fig. 1), the following values of thermal conductivity were used in the calculation:

$$K_1 = 600 \text{ Wm}^{-1}\text{K}^{-1}$$
$$K_2 = 0.0167 \text{ Wm}^{-1}\text{K}^{-1}$$
$$K_3 = 17.4 \text{ Wm}^{-1}\text{K}^{-1}.$$

In Fig. 6a, bulk thermal conductivity is presented as a function of volume fraction for the experimental parameter values given above, and for a highly-conductive interfacial layer ($K_2 = 10^{15}$ $\text{Wm}^{-1}\text{K}^{-1}$ in this calculation) and a strongly-resistive layer, $K_2 = 0.0$ $\text{Wm}^{-1}\text{K}^{-1}$. The results obtained here are in close agreement with those of [5], from which the values at $f = 0.4$ are also shown in Fig. 6a. The slight deviation of the curve for the conductive layer from the result of [5] at $f = 0.4$ is due to the difference in the microstructure for the two models. In Fig. 6b, calculated values of bulk thermal conductivity are shown for spheroidal particles with aspect ratios 0.5 and 2.0 and temperature gradient applied either perpendicular (F_x) or parallel (F_z) to the axis of rotation. For prolate spheroids with aspect ratio 2.0, the maximum achievable volume fraction on a simple-cubic lattice, $f_{\max}$ is $\pi/24$ and for oblate spheroids with aspect ratio 0.5, $f_{\max} = \pi/12$ [8]. Results for f up to these values are shown in Fig. 6b, although the curve for prolate spheroids with an x-directed temperature gradient cannot be distinguished from that for the oblate spheroids with the z-directed temperature gradient, so is not shown explicitly. The results from the equivalent inclusion model [5] are for spheroids with arbitrary distribution in space and orientation. It can be seen that the predictions from the equivalent-inclusion model are bounded by those of the simple-cubic lattice model in the case of prolate spheroids, but not for the oblate spheroids. Reduction of the bulk thermal conductivity below that of the matrix, as predicted in [5] for oblate spheroidal filler particles, is explained in terms of the important role of the particle size when thermal boundary resistances are present. The simple-cubic lattice calculation is carried out in terms of the *ratio* of the particle dimension to that of the unit cell and so does not cater for such size effects.

4. Conclusion

An analytical method has been developed to calculate the complex dielectric constant of composite materials with coated speroidal filler particles arranged on a simple-cubic lattice. Example calculations show good agreement with independent calculations and indicate features which may be exploited practically, for example optimization of the layer thickness to maximise dissipation of electromagnetic energy at a particular frequency. Calculations of bulk thermal conductivity also show good agreement with independent work.

Appendix: First multipole expansion coefficient

For spheroidal particles arranged on a simple-cubic lattice, the second-order tensor describing the bulk complex permittivity can be expressed as in (7). The independent components of the tensor can be obtained by solving two scalar problems in which the electric field is applied parallel to either x or z, and the particles replaced by singular, multipole sources. The first coefficient in the multipole expansion, b_{jj}^{000} with $j = x$ or z, is required to calculate ϵ_{jj} via (15). In this Appendix, analytical expressions for b_{jj}^{000} accurate to order $f^{14/3}$ are quoted.

Spheres

In the case of spherical particles, $b_{xx}^{000} = b_{zz}^{000}$ due to symmetry. If $\gamma = r_0/l$ with r_0 the particle radius and l the side length of the unit cell, the solution accurate to γ^7 is [2]

$$b_{xx}^{000} = 4\pi r_0^3 \left[\mathcal{L}_1^{-1} + \frac{4\pi r_0^3}{3\tau_0} - \frac{16(a'_{20})^2\gamma^{10}}{\mathcal{L}_3^{-1} + 20a'_{30}\gamma^7} - 176\mathcal{L}_5(a'_{30})^2\gamma^{14} + \mathcal{O}(\gamma^{18}) \right]^{-1}. \quad \text{(A1)}$$

The coefficients

$$a_{20} = 3.108227 \quad a_{30} = 0.5733293$$

arise in summing over the infinite number of lattice sites [11, table 13]. In the above equation, $a'_{nm} = l^{2n+1}a_{nm}$ and the function $\mathcal{L}_s$ in (A1) is obtained by applying continuity conditions at the interfaces between the particle core and layer domains and the interstitial domain. The derivation and definition is given in Section 2.4, Equation 24, although the superscript 23 is dropped here.

Spheroids

For a system of prolate spheroidal particles as shown in Fig. 1, applying an electric field parallel to x yields [6]

$$b_{xx}^{000} = 4\pi d^3 \left\{ s_1\left(\mathcal{L}_1^1\right)^{-1} + \frac{4\pi d^3}{3\tau_0} + 4a'_{20}s_2\lambda^5 + 2a'_{30}s_3\lambda^7 + C\left(24a'_{20}\lambda^5 + 120a'_{30}s_2\lambda^7\right) - 6a'_{30}\lambda^7\left[\chi - s_4\left(\chi - 2a'_{30}s_5\lambda^7\right)\right] + \mathcal{O}(\lambda^{18}) \right\}^{-1}, \quad \text{(A2)}$$

with

$$C = -\frac{s_6\left(\mathcal{L}_3^1\right)^{-1} + 4a'_{20}s_7\lambda^5 + 2a'_{30}s_8\lambda^7}{6\left[s_9\left(\mathcal{L}_3^1\right)^{-1} + 20a'_{30}s_7\lambda^7\right]}, \quad \text{(A3)}$$

and

$$\chi = s_{10} + 6Cs_{11} + 20a'_{30}s_{12}\mathcal{L}_5^1\lambda^7. \quad \text{(A4)}$$

In the above equations, $2d$ is the interfocal length of the spheroids and $\lambda = d/l$. The constants s_j, $j = 1, \ldots, 12$ arise in transforming from spherical to spheroidal harmonics. This operation is required in order to match the multipole solution expressed in terms of spherical harmonics, discussed in Section 2.3, with the interstitial domain solution expressed in terms of spheroidal harmonics. The details of the transformation and determination of the relevant matrix elements are given elswhere [6, 8]. The numerical values of the s_j are

$s_1 = -1.500$	$s_7 = 0.1333$
$s_2 = -1.800$	$s_8 = 1.111$
$s_3 = -9.643$	$s_9 = -4.375$
$s_4 = 3.500$	$s_{10} = 0.02550$
$s_5 = 1.333$	$s_{11} = 0.5339$
$s_6 = -0.5838$	$s_{12} = 0.007037.$

The function $\mathcal{L}_s^t$ in (A2) is obtained by applying continuity conditions at the interfaces between the particle core and layer domains and the interstitial domain. The derivation and definition is given in Section 2.4

If the electric field is applied parallel to z, the result is [6]

$$b_{zz}^{000} = 4\pi d^3 \left\{ \Gamma_1\left(\mathcal{L}_1^0\right)^{-1} + \frac{4\pi d^3}{3\tau_0} + 4a'_{20}\Gamma_2\lambda^5 + 6a'_{30}\Gamma_3\lambda^7 - \frac{\left[4a'_{20}\Gamma_6\left(\mathcal{L}_3^0\right)^{-1}\lambda^5 + 2a'_{30}\Gamma_7\left(\mathcal{L}_3^0\right)^{-1}\lambda^7 + 16(a'_{20})^2\Gamma_8\lambda^{10} + 8a'_{20}a'_{30}\Gamma_9\lambda^{12} + 12(a'_{30})^2\Gamma_{10}\lambda^{14}\right]}{\left[\Gamma_{11}\left(\mathcal{L}_3^0\right)^{-1} + 20a'_{30}\Gamma_8\lambda^7\right]} - (a'_{30})^2\left[36\Gamma_4\mathcal{L}_5^0 + 140\Gamma_5\mathcal{L}_5^4\right]\lambda^{14} + \mathcal{O}(\lambda^{18}) \right\}^{-1}. \quad \text{(A5)}$$

Similarly to the s_j in (A2), the constants Γ_j, $j = 1, \ldots, 11$ in (A5) arise in transforming from spherical to spheroidal harmonics. The numerical values are

$$\begin{aligned} \Gamma_1 &= 3.000 & \Gamma_7 &= -97.56 \\ \Gamma_2 &= 0.6000 & \Gamma_8 &= 0.4 \\ \Gamma_3 &= 0.1947 & \Gamma_9 &= 5.056 \\ \Gamma_4 &= 0.001466 & \Gamma_{10} &= 4.137 \\ \Gamma_5 &= 0.03694 & \Gamma_{11} &= 17.5 \\ \Gamma_6 &= -10.48 \end{aligned}$$

Equations (A2) and (A5) are in a form which is appropriate for prolate spheroids. The correct form for oblate spheroids is obtained directly from these equations on replacing d with $-id$.

References

1. G. K. BATCHELOR, *Ann. Rev. Fluid Mech.* **6** (1974) 227.
2. M. ZUZOVSKY and H. BRENNER, *J. Appl. Math. Phys.* **28** (1977) 979.
3. R. C. MCPHEDRAN and D. R. MCKENZIE, *Proc. Roy. Soc. Lond A.* **359** (1978) 45.
4. I. J. YOUNGS, in Proceedings of BEMC 99, the 9th International Conference on Electromagnetic Measurement, Brighton, November 1999, p. 53 and submitted to *IEE Proc. Sci. Meas. Technol*.
5. M. L. DUNN and M. TAYA, *J. Appl. Phys.* **73** (1993) 1711.
6. N. HARFIELD, *J. Phys. D: Appl. Phys.* **32** (1999) 1104.
7. A. S. SANGANI and C. YAO, *J. Appl. Phys.* **63** (1988) 1334.
8. N. HARFIELD, *Eur. Phys. J. AP* **6** (1999) 13.
9. J. C. MAXWELL, "A Treatise on Electricity and Magnetism" (Clarendon, Oxford, 1881).
10. H.HASIMOTO, *J. Fluid Mech.* **5** (1959) 317.
11. A. S. SANGANI, PhD Thesis, Stanford University, 1983.
12. J. A. STRATTON, "Electromagnetic Theory" (McGraw-Hill, New York, 1941).
13. R. PELSTER and U. SIMON, *Colloid Polym. Sci.* **277** (1999) 2.
14. A. R. VON HIPPEL, "Dielectrics and Waves" (John Wiley, New York, 1954).

Received 5 January
and accepted 2 May 2000